Improved Quantum Efficiency of Highly Efficient Perovskite $BaSnO_3$-Based Dye-Sensitized Solar Cells

Seong Sik Shin,[†,‡] Ju Seong Kim,[†,‡] Jae Ho Suk,[†,‡] Kee Doo Lee,[§,⊥] Dong Wook Kim,[∥] Jong Hoon Park,[†] In Sun Cho,[#] Kug Sun Hong,[†,‡,*] and Jin Young Kim[§,⊥,*]

[†]Department of Materials Science and Engineering, Seoul National University, Seoul, 151-744, Korea, [‡]WCU Hybrid Materials Program, Department of Materials Science and Engineering, Seoul National University, Seoul, 151-744, Korea, [§]Photo-electronic Hybrid Research Center, Korea Institute of Science and Technology, Seoul 136-791, Korea, [⊥]Green School, Korea University, 145, Anam-ro, Seongbuk-gu, Seoul 136-701, Korea, [∥]Department of Chemistry, Northwestern University, 245 Sheridan Road, Evanston, Illinois 60208, United States , and [#]Department of Mechanical Engineering, Stanford University, Stanford, California 94305, United States

ABSTRACT Ternary oxides are potential candidates as an electron-transporting material that can replace TiO_2 in dye-sensitized solar cells (DSSCs), as their electronic/optical properties can be easily controlled by manipulating the composition and/or by doping. Here, we report a new highly efficient DSSC using perovskite $BaSnO_3$ (BSO) nanoparticles. In addition, the effects of a $TiCl_4$ treatment on the physical, chemical, and photovoltaic properties of the BSO-based DSSCs are investigated. The $TiCl_4$ treatment was found to form an ultrathin TiO_2 layer on the BSO surface, the thickness of which increases with the treatment time. The formation of the TiO_2 shell layer improved the charge-collection efficiency by enhancing the charge transport and suppressing the charge recombination. It was also found that the $TiCl_4$ treatment significantly reduces the amount of surface OH species, resulting in reduced dye adsorption and reduced light-harvesting efficiency. The trade-off effect between the charge-collection and light-harvesting efficiencies resulted in the highest quantum efficiency (*i.e.*, short-circuit photocurrent density), leading to the highest conversion efficiency of 5.5% after a $TiCl_4$ treatment of 3 min (*cf.* 4.5% for bare BSO). The conversion efficiency could be increased further to 6.2% by increasing the thickness of the BSO film, which is one of the highest efficiencies from non-TiO_2-based DSSCs.

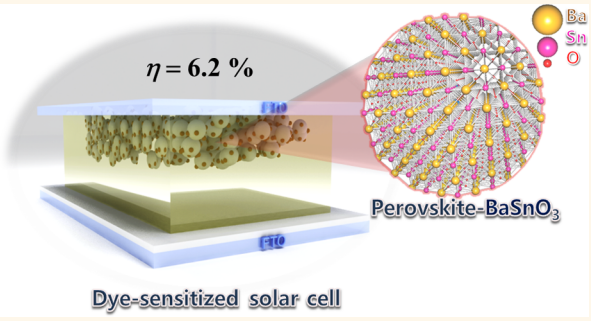

KEYWORDS: barium stannate · perovskite · dye-sensitized solar cell · quantum efficiency · electron transport/recombination

Dye-sensitized solar cells (DSSCs) have received much attention owing to their low fabrication cost and remarkable conversion efficiency.[1,2] A DSSC is typically composed of a sensitizer, an electron-transporting phase, a hole-transporting phase, and current-collecting substrates. Among them, the electron-transporting phase, mostly a mesoporous electrode consisting of wide-band-gap nanoparticles, is one of the key components governing the device performance, as it directly influences several working mechanisms of the DSSC including dye adsorption,[3] photoelectron injection,[4] light scattering,[5,6] and electron transport/recombination.[7,8] The most commonly used and the best wide-band-gap material thus far is TiO_2.[2] To date, therefore, most relevant studies have focused on either modifying the TiO_2 electrode or optimizing other components (*e.g.*, electrolyte and/or dye molecules) according to the property of TiO_2 nanoparticle films. On the other hand, the sole use of TiO_2 has limited the selection of other components. For instance, small semiconductor quantum dots occasionally cannot be used as a sensitizer for a TiO_2 electrode, as their conduction band (or LUMO) level is lower than that of TiO_2, and thus the excited photoelectrons cannot be injected from the sensitizer to TiO_2.[9] Therefore, finding new alternatives to TiO_2 capable of comparable or better device performance can open up new possibilities for further improving the performance of DSSCs.

The search for an alternative started from the binary oxide n-type semiconductors of

* Address correspondence to kimjy@kist.re.kr, kshongss@plaza.snu.ac.kr.

Received for review August 6, 2012 and accepted January 8, 2013.

Published online January 15, 2013
10.1021/nn305341x

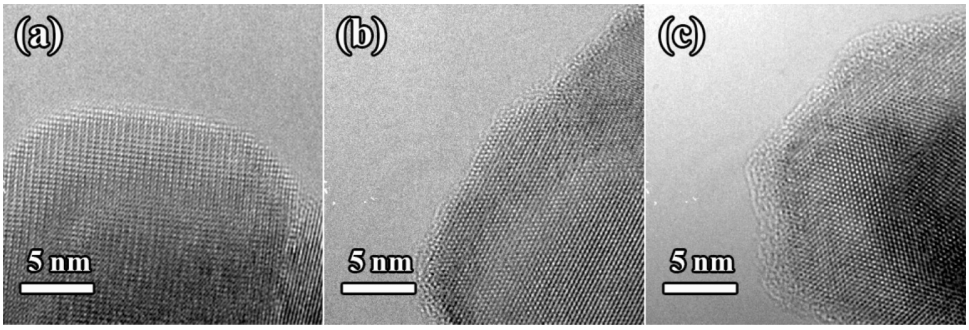

Figure 1. HR-TEM images of BSO nanoparticles immersed in a $TiCl_4$ aqueous solution ($TiCl_4$ treatment) for different immersion times: (a) 0 min, (b) 3 min, and (c) 10 min.

ZnO,[10,11] SnO_2,[12,13] and Nb_2O_5[14] due to their analogy with TiO_2, but none of them exhibited comparable device performances. Ternary oxide semiconductors are better candidates than binary oxides, as their chemical properties and band structure can easily be modified by altering the composition. However, ternary oxide semiconductors have not been investigated intensively, and the only a few examples (*e.g.*, Zn_2SnO_4[15,16]) have demonstrated functioning DSSCs (>2%). Recently, there have been a couple of reports on the photovoltaic properties of $BaSnO_3$ (BSO)-based DSSCs. Zhang *et al*. reported that dye-sensitized BSO could be used as a photoanode of DSSCs,[17] and Tang *et al*. reported the synthesis of one-dimensional BSO hollow architectures with a length of 1.5−5 μm as a photoelectrode of DSSCs.[18] However, the device performance of BSO-based DSSCs as reported thus far is very poor, exhibiting conversion efficiencies lower than 1.1%.

In this study, ternary BSO is investigated as an electron-transporting material of a highly efficient DSSC. BSO is an n-type semiconductor with a wide band gap of 3.1 eV,[19] and its band structure and electrical properties can be controlled easily by atomic substitution or doping into the Ba or Sn site.[20,21] The effect of a $TiCl_4$ treatment on the physical and chemical properties of the BSO electrode was investigated systematically by means of electron microscopy and other surface-chemistry characterization tools. A comprehensive investigation of the electron dynamics (by photocurrent/voltage spectroscopy) and the quantum efficiency revealed that the physical/chemical modification of the BSO surface significantly influences the DSSC performance, such as the light-harvesting and charge-collection capabilities. As a result, the optimal treatment improved the conversion efficiency by 22% (from 4.5% to 5.5%). Moreover, the efficiency could be increased further to 6.2% by changing the thickness of the BSO electrode.

RESULT AND DISCUSSION

Characterization of the Chemically Treated BSO Films. Our preliminary experiments with a scanning electron microscope (SEM) and X-ray diffraction (XRD) (Figure S1 in the Supporting Information) showed that a $TiCl_4$ treatment lasting up to 10 min has essentially no effect on the morphological and crystalline properties of the BSO film macroscopically (or on a relatively large scale). Therefore, the nanoscale morphology of the samples was investigated using high-resolution transmission electron microscopy (HR-TEM). Figure 1 compares high-resolution images of the BSO nanoparticles treated for various amounts of time. The high-resolution images of the BSO films treated with a $TiCl_4$ solution (*i.e.*, Figure 1b, c) combined with the elemental mapping results (Figure S2 in the Supporting Information) provide clear evidence of the formation of TiO_2 shell layers. The 3 min $TiCl_4$ treatment forms an ultrathin shell layer (<1 nm) on the surface of BSO, and its thickness increases to 2−3 nm when the treatment continues for 10 min (Figure 1c). An elemental analysis (Figure S2 in the Supporting Information) also shows that the same samples exhibit a homogeneous distribution of Ba, Sn, and Ti, indicating the uniform formation of Ti-containing layers (presumably TiO_2) created by the $TiCl_4$ treatment. Although a $TiCl_4$ treatment is generally known to produce TiO_2 layers with the rutile[22] or anatase crystalline phase,[23] the selected-area electron diffraction (SAED) patterns (Figure S3 in the Supporting Information) reveal that the TiO_2 thin layers are amorphous. This result, which is consistent with the XRD result (Figure S1e in the Supporting Information), can be ascribed to the thinness of the TiO_2 layer (<3 nm), caused by the short treatment time (<10 min).

Figure 2 displays the X-ray photoelectron spectroscopy (XPS) spectra of BSO films treated with $TiCl_4$ for various times ranging from 0 to 10 min. No Ti was noted in the bare BSO (Figure 2a), whereas the Ti 2p spectra exhibit two characteristic peaks at 458 and 464 eV upon $TiCl_4$ treatment. The intensity of the peaks gradually increases with time, suggesting that the amount of TiO_2 also increases with the treatment time. A quantitative analysis of the XPS spectra revealed that the atomic percent of Ti is 0%, 1.6%, 2.1%, 3.0%, and 6.0% for the BSO films immersed in a $TiCl_4$ aqueous solution for 0, 1, 3, 5, and 10 min, respectively. This result is consistent with the TEM results (Figure 1), where

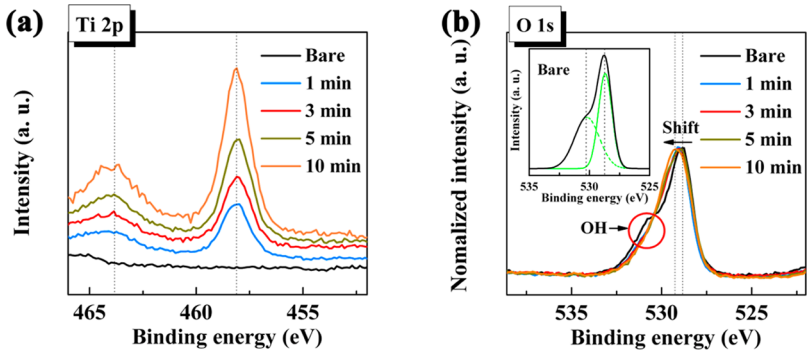

Figure 2. XPS spectra of BSO films prepared under various $TiCl_4$ treatment times: (a) Ti 2p and (b) O 1s.

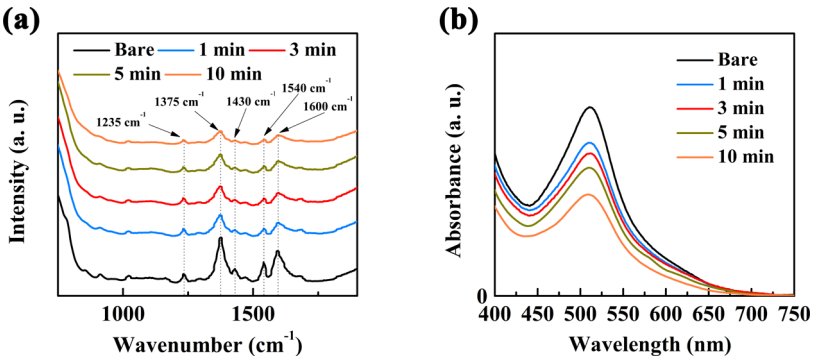

Figure 3. (a) ATR-FTIR spectra of a dye (N719) adsorbed on BSO films prepared under various $TiCl_4$ treatment times and (b) UV−vis absorption spectra of the dye (N719) detached from the BSO films prepared under various treatment times. To measure UV−vis absorption spectra of the dye (N719), the dye was desorbed by a NH_4OH solution in water and ethanol (50:50, v/v).

the thickness of the TiO_2 shell layer increases with a longer treatment time. Figure 2b shows the normalized O 1s spectra of the samples, where the inset shows the spectrum of the bare BSO only. A peak deconvolution process (inset of Figure 2b) clearly shows that the O 1s spectrum of the bare BSO is composed of two peaks, at 528.7 and 530.3 eV. This phenomenon is often observed in $ASnO_3$ perovskite oxide compounds, as OH species can easily adsorb onto the surface of $ASnO_3$ oxides.[24,25] A peak with lower binding energy (*i.e.*, at 528.7 eV) is usually associated with the contribution of O_2^- ions in the perovskite anionic network, whereas one with higher binding energy (*i.e.*, at 530.3 eV) can be ascribed to the oxygen atoms in the OH species and/or the adsorbed oxygen species on the surface.[24,25] Therefore, it can be concluded that a significant amount of OH species is adsorbed on the surface of the BSO. After the $TiCl_4$ treatment, however, the shoulder peak at 530.3 eV essentially disappears even after a treatment lasting only for 1 min. This result indicates that the $TiCl_4$ treatment and the resulting formation of the TiO_2 shell layer effectively reduce the amount of OH species adsorbed on the BSO surface. It is also notable that the position of the peak at a lower binding energy gradually shifts toward a higher energy level, which may result from the increasing contribution by the lattice oxygen in the TiO_2 (at 529.6 eV).[26]

Optical Analysis of Dye-Loaded BSO Films. Figure 3 shows the effect of the $TiCl_4$ treatment on the adsorption of N719 dye molecules on the BSO electrode. The peaks in the attenuated total reflectance FT-IR (ATR-FTIR) spectra of BSO films after the adsorption of the dye (Figure 3a) are located at the same position as those in the dye-sensitized TiO_2,[27] suggesting that the adsorption mechanism of N719 dye molecules on BSO is similar to that on TiO_2. It is notable that the spectra show a strong peak at 1375 cm^{-1}, which is generally indicative of the strong binding of N719 dye molecules *via* the formation of a bidentate chelate.[28] No evidence of free carboxylic acid (*e.g.*, a C═O elongation peak at 1735 cm^{-1}) was found in the IR spectra. Stronger bidentate chelation (peak at 1375 cm^{-1}) compared to nonbidentate chelation (peak at 1735 cm^{-1}) is known to be beneficial to the chemical stability of adsorbed dyes and the charge injection from dye molecules to oxides.[27,29,30] After the $TiCl_4$ treatment, however, the intensity of the peaks associated with dye adsorption significantly decreases, suggesting that the number of dye molecules adsorbed on the BSO decreases with the $TiCl_4$ treatment. The effect of the $TiCl_4$ treatment on the amount of adsorbed dye molecules was investigated further using UV−vis spectroscopy (Figure 3b). The spectra were obtained after the dye desorption process in a basic solution. The intensity of the absorption peak by dye molecules at 512 nm decreases with the $TiCl_4$ treatment and with time, from which the numbers of adsorbed dye molecules for bare

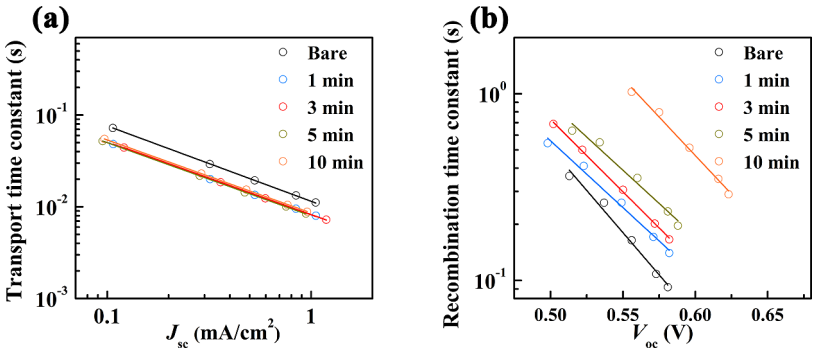

Figure 4. (a) Electron transport (IMPS) time constant as a function of the short-circuit current density and (b) the electron recombination (IMVS) time constant as a function of the open-circuit voltage for BSO-based DSSCs with various $TiCl_4$ treatment times.

and 1, 3, 5, and 10 min samples are determined to be 2.94×10^{-8}, 2.36×10^{-8}, 2.19×10^{-8}, 1.95×10^{-8}, and 1.51×10^{-8} moles, respectively. This result is qualitatively consistent with the ATR-FTIR spectroscopy result. Therefore, it can be concluded that the $TiCl_4$ treatment decreases the amount of dye adsorption on the BSO film. This conclusion may seem to be somewhat counterintuitive given that the $TiCl_4$ treatment is known to increase the amount of dye adsorption for TiO_2-based DSSCs.[31,32] This controversy can be addressed in terms of the surface hydroxyl group. The existence of a hydroxyl group (or OH species) on the surface of TiO_2 (or BSO) is essential for the chemisorption of dye molecules with carboxylic functional groups.[33,34] From the XPS analysis (Figure 2b), it was found that the $TiCl_4$ treatment effectively reduces the amount of surface OH species of BSO. Therefore, the reduced dye adsorption can be attributed to the reduced OH species by the $TiCl_4$ treatment. The formation of an additional TiO_2 layer as a result of the $TiCl_4$ treatment may, in principal, reduce the total internal surface area of the electrode, which can lead to reduced dye adsorption. However, the pore size analysis (Figure S4 in the Supporting Information) showed that the pore structure is essentially unchanged by the $TiCl_4$ treatment.

Effect of a Chemical Treatment on the Electron Dynamics and Light-Harvesting Capabilities. Figure 4 shows the effect of the $TiCl_4$ treatment on the electron dynamics of BSO-based DSSCs measured by intensity-modulated photocurrent/photovoltage spectroscopy (IMPS/IMVS). All samples show a typical power-law dependence of transport time constants on the J_{sc} value (Figure 4a), indicating an exclusive random walk of photoelectrons between trap sites that have a power-law distribution of waiting (release) times in the form of $\tau^{-1-\alpha}$, where the parameter α can be related to the shape of the trap distribution.[35,36] The best fit of the data from the bare BSO DSSC yields a slope of -0.82 (arbitrary unit), which is significantly steeper than that of the conventional TiO_2 nanoparticle counterpart (-0.67, Figure S5 in the Supporting Information). The slope of the fitted line is usually correlated with the α value, according to the following equation.

$$D = C_1 N_{tot}^{1/3\ -\ 1/\alpha} n^{1/\alpha\ -\ 1} \quad (1)$$

Here, N_{tot} is the total density of the transport-limiting traps, n is the photoelectron density, and C_1 is a constant. The diffusion coefficient is generally inversely proportional to the transport (or collection) time constant ($D = L^2/2.35\tau_c$; L, film thickness),[36,37] and the photoelectron density can be represented by J_{sc} ($n \propto J_{sc}\tau_r$).[38] Therefore, a steeper slope (*i.e.*, a smaller value of α) of the bare BSO DSSC may indicate that the average trap energy in the trap distribution (or the average residence time of trapped electrons) of BSO is higher (or longer) compared to when TiO_2 is used.[36] The best fit of the data from $TiCl_4$-treated DSSCs exhibits slightly smaller (or less negative) slopes ranging from -0.79 to -0.80 regardless of the duration of the treatment. Such a small change in the slope (*i.e.*, the α value) indicates that the $TiCl_4$ treatment essentially does not alter the overall density and distribution of transport-limiting traps. Despite the fact that the distribution of traps is essentially unaffected by the $TiCl_4$ treatment, the transport time constant of the BSO-based DSSCs decreases by approximately 30% in the entire range of the J_{sc} (*i.e.*, photoelectron density) after the $TiCl_4$ treatment regardless of the duration. The modest acceleration of photoelectrons by the $TiCl_4$ treatment can be ascribed to a couple of factors. First, the formation of very thin TiO_2 layers, particularly at the interparticle interfaces, can facilitate the charge transport between BSO nanoparticles. Given that the sintering temperature during the device fabrication process (500 °C) is much lower than the temperature for the synthesis of BSO nanoparticles (900 °C), it is possible that the physical connection (or necking) between the BSO nanoparticles is not the best. Therefore, the $TiCl_4$-induced TiO_2 layer between the BSO nanoparticles can lead to improved physical connectivity and thus faster interparticle charge transport. However, for some reason, such enhancement appears even with very short treatment time, as the transport time does not decrease further with an increase in the treatment time. Second,

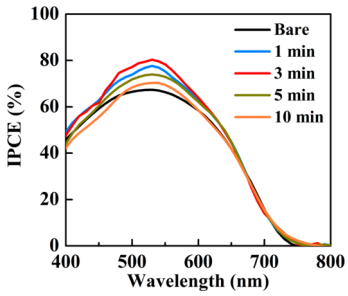

Figure 5. Incident photon-to-current conversion efficiency (IPCE) spectra of BSO-based DSSCs with various $TiCl_4$ treatment times.

the $TiCl_4$ treatment may deactivate (or passivate) some of the transport-limiting traps located at the outermost surface of the BSO nanoparticles (*i.e.*, surface states). According to eq 1, the reduced number of transport-limiting traps (N_{tot}) leads to faster charge transport (D) due to the negative exponent of N_{tot} ($1/3 - 1/\alpha$, where $0 < \alpha < 1$). Therefore, the transport can accelerate due to the $TiCl_4$ treatment. This hypothesis is in quantitative agreement with the slightly reduced slope of the IMPS data due to the $TiCl_4$ treatment. Figure 4b displays the effect of the $TiCl_4$ treatment on the charge recombination property of BSO-based DSSCs. The recombination time constants increase monotonically with an increase in the duration of the $TiCl_4$ treatment. The formation of TiO_2 shell layers on the surfaces of BSO nanoparticles can prevent the reaction of injected photoelectrons with the oxidized species (I_3^-) in the electrolyte by physically separating them. In addition, the higher conduction band edge position of TiO_2 (likely in the form of TiO_2) compared to that of BSO will repulse the electrons toward the BSO side owing to the energetics. As evidenced by the TEM images (Figure 1) and the XPS analysis result (Figure 2), the amount of TiO_2 and thus its thickness both increase with the time. Therefore, the electron recombination from the BSO core nanoparticle to the electrolyte through the TiO_2 shell layer should become slower with an increase in the duration of the $TiCl_4$ treatment. The charge-collection efficiency is often calculated from the transport and recombination time constants measured by IMPS/IMVS, but in this study, the actual value under the working conditions cannot be calculated because the transport and recombination time constants were measured at short-circuit and open-circuit conditions, respectively. However, it is reasonable to conclude from the transport/recombination time constants that the charge-collection efficiency increases with the $TiCl_4$ treatment and with an increase in the treatment time.

Figure 5 displays the IPCE spectra of the BSO-based DSSCs. All DSSCs show the typical spectral response of N719-based DSSCs with a peak at around 530 nm. However, the maximum IPCE (or external quantum efficiency; EQE) varies with the condition of the $TiCl_4$ treatment. The DSSC with a 3 min treatment exhibits the highest maximum EQE, whereas the bare BSO DSSC shows the lowest maximum EQE. The short-circuit current density (J_{sc}) calculated from the integrated area of the IPCE spectra is 9.95, 11.52, 12.58, 11.06, and 10.01 mA/cm^2 for the bare, 1 min, 3 min, 5 min, and 10 min samples, respectively. The calculated value of J_{sc} shows the same trend as the maximum EQE. The IPCE value can be expressed by the following equation.

$$\text{IPCE} = \eta_{lh}\eta_{inj}\eta_{cc} \quad (2)$$

Here, η_{lh}, η_{inj}, and η_{cc} represent the light-harvesting, charge-injection, and charge-collection efficiencies. The light-harvesting efficiency is usually assumed to be proportional to the amount of dye loading.[39] From the conclusion of the FT-IR and UV−vis spectroscopy (Figure 3), the amount of dye loading drops significantly with the $TiCl_4$ treatment of only 1 min (*cf.* bare BSO) and further decreases gradually as the treatment time increases from 1 min to 3 min. Then, the amount of dye loading significantly drops again between 5 min and 10 min. Therefore, it can be concluded that the light-harvesting efficiency decreases upon $TiCl_4$ treatment and keeps decreasing with an increase in the treatment time. On the other hand, the IMPS/IMVS study (Figure 4) revealed that the charge-collection efficiency increases with the $TiCl_4$ treatment and with an increase in the treatment time. The trade-off of the effects of the light-harvesting and charge-collection efficiencies could lead to their highest product (*i.e.*, the highest IPCE value) around the midpoint (*i.e.*, 3 min). It should be noted that the effect of the charge-injection efficiency on the IPCE spectra is not considered in this study because it is premature to discuss the charge-injection efficiency without proper measurements, for instance by transient absorption spectroscopy.

DSSC Performance and Dark Current. Figure 6a shows the photocurrent density−voltage (J−V) curves of the BSO-based DSSCs under simulated solar illumination (100 mW/cm^2, AM 1.5G). The solar cell parameters are summarized in Table 1. No effort other than the $TiCl_4$ treatment was made to optimize the DSSC performance. The J_{sc} value increases with the duration of the $TiCl_4$ treatment, reaching the maximum value of 13.96 mA/cm^2 at 3 min, after which it gradually decreases with time. This result is in good agreement with the IPCE spectra (Figure 5), which has been ascribed to the trade-off effect of the increased charge-collection efficiency and the decreased light-harvesting efficiency. The open-circuit voltage (V_{oc}) increases monotonically from 0.61 to 0.68 V over time from 0 min (bare) to 10 min. As concluded from the TEM images (Figure 1) and the XPS data (Figure 2a), the $TiCl_4$ treatment forms a very thin TiO_2 layer on the surface of the BSO particles, and its thickness increases to 2−3 nm (10 min). The conduction band edge of TiO_2 (−0.5 eV *vs* NHE)[40] is higher (*i.e.*, more negative) than that of BSO (−0.2 to −0.4 eV *vs* NHE).[41] Therefore, the back-electron transfer from BSO to the

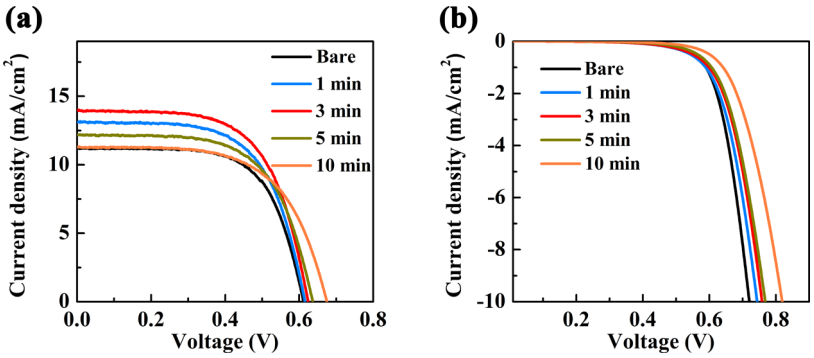

Figure 6. (a) Photocurrent density−voltage curves measured under AM 1.5G, at 1 sun light intensity with a shadow mask. (b) Dark-current density of BSO-based DSSCs with various $TiCl_4$ treatment times.

TABLE 1. Photocurrent Density−Voltage Characteristics of BSO-Based DSSCs with Various $TiCl_4$ Treatment Times

	J_{sc} (mA/cm^2)	V_{oc} (V)	FF	η (%)
bare	11.19	0.61	0.66	4.5
1 min	13.11	0.62	0.63	5.1
3 min	13.96	0.62	0.63	5.5
5 min	12.19	0.64	0.63	4.9
10 min	11.31	0.68	0.61	4.7

oxidized species (I_3^-) in the electrolyte becomes energetically difficult, leading to fewer recombinations and increased V_{oc} values.[42,43] The dark $J-V$ curves (Figure 6b) also reveal that the $TiCl_4$ treatment suppresses the dark current (*i.e.*, the back-electron transfer), shifting its onset toward a higher forward bias.[31] In addition, the formation of the TiO_2 layer with the conduction band edge higher than that of BSO can cause the upward movement of the band edge, resulting in a higher V_{oc} value.[44] On the other hand, the fill factor decreases monotonically from 0.66 to 0.61 with an increase in the time from 0 min (bare) to 10 min. This phenomenon (*i.e.*, reduced fill factor after the $TiCl_4$ treatment) has been reported by others[31] and ascribed to the resistance of FTO and the increased photocurrent. This explanation does not apply to this study because the photocurrent density actually decreases after 3 min. One can obtain better insight into the fill factor from the analysis of the dark-current density (J_d). The dark $J-V$ characteristics can be described using the following diode equation.

$$J_d = J_0[\exp(qV/mkT) - 1] \quad (3)$$

In this equation, q is the elementary charge, V is the applied voltage, k is the Boltzmann constant, T is the temperature, m is the diode ideality factor, and J_0 is the exchange current density in the dark. It was recently reported that m and J_0 significantly affect the fill factor,[45] where the reduced fill factor was associated with increased values of m and J_0. The best fit of the dark $J-V$ curves of the bare-BSO DSSC yields m and J_0 values of 1.93 and 6.7 $\times$ 10^{-6} mA/cm^2, respectively,

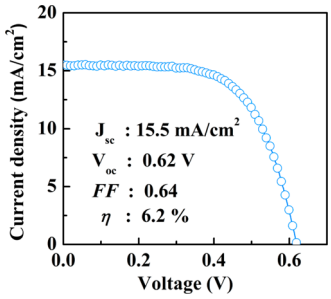

Figure 7. Photocurrent density−voltage curve of an optimized DSSC fabricated from a BSO film immersed in a $TiCl_4$ aqueous solution for 3 min measured under AM 1.5G, at 1 sun light intensity with a shadow mask.

whereas the DSSC treated for 10 min yields 2.38 and 2.7 $\times$ 10^{-5} mA/cm^2 (Figure S6 in the Supporting Information). Therefore, the decreased fill factor of $TiCl_4$-treated BSO DSSCs may be associated with their dark $J-V$ characteristics (*i.e.*, an increased diode ideality factor and increased exchange current density). Owing to the opposite dependence of V_{oc} and the fill factor on the $TiCl_4$ treatment, the overall conversion efficiency follows the trend of J_{sc}, exhibiting the highest value of 5.5% after a treatment of 3 min.

Optimized DSSC Performance. The device performance can be improved further by manipulating the fabrication process. Figure 7 shows the $J-V$ curve of a DSSC consisting of a 32 μm thick BSO film with a $TiCl_4$ treatment of 3 min. The J_{sc} value is increased to 15.5 mA/cm^2, whereas the V_{oc} and the fill factor remain similar to those of the thinner counterpart (the 3 min sample shown in Figure 6 and Table 1), resulting in a high conversion efficiency of 6.2%. Thus far, to the best of our knowledge, this is one of the highest efficiencies reported for non-TiO_2-based DSSCs. It should be noted that the experimental results are quite reproducible, showing a deviation of less than 5% (Table S1 in the Supporting Information).

CONCLUSION

In summary, highly efficient perovskite BSO-based DSSCs were demonstrated with the aid of a $TiCl_4$

treatment. The $TiCl_4$ treatment was found to affect the physical, chemical, and photovoltaic properties of BSO-based DSSCs. The $TiCl_4$ treatment formed an amorphous TiO_2 layer on the BSO surface and reduced the amount of the surface OH species, resulting in increased charge-collection efficiency and decreased light-harvesting efficiency, respectively. The increased charge-collection efficiency is ascribed to the enhanced interparticle connectivity and the reduced back electron transfer caused by the TiO_2 shell layer. The decreased light-harvesting efficiency is attributed to the reduced dye loading in the presence of the TiO_2 shell layer. As a result, the highest external quantum efficiency (or IPCE) was obtained when the BSO film was treated with a $TiCl_4$ solution for 3 min. The J_{sc} value followed the same trend as the IPCE, showing the highest value when treated for 3 min. The V_{oc} increased with the $TiCl_4$ treatment owing to the negative (or upward) band-edge movement caused by the formation of the ultrathin TiO_2 shell layers. On the other hand, the fill factor decreased with the $TiCl_4$ treatment, which is ascribed to the increased diode ideality factor and exchange current density in the dark. As a result, the BSO-based DSSCs, after the $TiCl_4$ treatment for 3 min, exhibited the highest conversion efficiency of 5.5%, which is 22% higher than that of the bare-BSO DSSC (4.5%). The conversion efficiency could be improved further to 6.2% after adjusting the electrode thickness. This efficiency is, to the best of our knowledge, one of the highest reported efficiencies of DSSCs without using TiO_2 nanoparticles. This result will encourage researchers to explore new multicomponent oxides for the replacement of TiO_2 in DSSCs.

METHODS

Synthesis of BSO Nanoparticles. All chemicals for the preparation of nanoparticles were of reagent grade and were used without further purification. Monodispersed $BaSnO_3$ nanoparticles were synthesized as follows. A 10 mmol amount of $BaCl_2 \cdot 2H_2O$ (Sigma-Aldrich, 99%) and $SnCl_4 \cdot 5H_2O$ (Sigma-Aldrich, 98%) were dissolved in H_2O_2 (30 wt %) under vigorous magnetic stirring, and citric acid was then introduced into the transparent mixing solution. Then, 120 mL of aqueous NH_4OH was added to the reaction solution. White, amorphous precipitates were formed immediately, and this solution, including the precipitates, was magnetically stirred for 12 h at room temperature. The obtained products were thoroughly washed with distilled water by centrifugation and were then finally freeze-dried. The dried amorphous precursor was calcined at 900 °C for 2 h in air.

Preparation of BSO Films. Porous BSO films were prepared on fluorine-doped tin oxide (FTO) glass substrates from a home-made paste including BSO nanoparticles *via* a doctor-blade method. The coated films were annealed under an ambient atmosphere following multiple heating steps (325 °C for 5 min, 375 °C for 5 min, 450 °C for 15 min, and then 500 °C for 15 min). For the $TiCl_4$ treatment, the annealed BSO films were immersed in a 0.05 M $TiCl_4$ aqueous solution for various times (0, 1, 3, 5, and 10 min) at 50 °C. Then, the films were sintered again at 500 °C for 30 min.

DSSC Assembly. For the dye adsorption, the BSO films with (or without) the $TiCl_4$ treatment were soaked in a dye solution (0.5 mM purified N719 dye in absolute ethanol) at room temperatures for 60 min. In this case, the soaking time for the BSO films is much shorter than that for conventional materials (*e.g.*, 20 h for TiO_2) due to the fast dye adsorption kinetics on the BSO surface. After the dye adsorption process, the films were thoroughly rinsed with a mild stream of absolute ethanol to remove the physically adsorbed dye molecules. Sandwich-type DSSCs were then assembled using the dye-adsorbed BSO film and a platinized FTO substrate (by sputtering) with a hot-melt film (~60 μm, Surlyn) between them. Finally, an iodide-based liquid electrolyte (SI16 L1535-01, Merck) was infiltrated into the cell through a hole from the counter electrode side. The active area of the dye-coated BSO film was 0.16 cm^2. A schematic illustration describing the overall fabrication process is presented in the Supporting Information (Scheme S1).

Material and DSSC Characterization. The crystal structure of the materials was characterized using an X-ray powder diffractometer (XRD; New D8 Advance, Bruker). The morphological properties of the films were investigated using a field-emission scanning electron microscope (SU 70, Hitachi) and a high-resolution transmission electron microscope (JEM 3000F, JEOL). The pore size distribution of the nanoporous films was measured by a Brunauer–Emmett–Teller surface area analyzer (BELSORP-mini II, BEL). XPS spectra were collected using an ESCA spectrometer (Al Kα X-ray source, Sigma Probe) when the measured binding energy was calibrated with contaminated carbon (C 1s peak at 284.5 eV). The dye-adsorption mechanism was investigated with the aid of an ATR-FTIR spectrometer (Nicolet 6700, Thermo Scientific), and optical properties of the samples were characterized using a UV–vis spectrometer (LAMBDA 650, PerkinElmer). The photocurrent–voltage characteristics of the DSSCs were measured with a potentiostat (CHI 608C, CH Instruments) under simulated 1 sun illumination (AM 1.5, 100 mW/cm^2). The IPCE spectra were obtained in the range 400–800 nm using a specially designed IPCE system (K 3100, McScience) for DSSCs. An electrochemical workstation (Zennium, Zahner) with an attached frequency response analyzer and a light-emitting diode (667 nm) was utilized for the intensity-modulated photocurrent/photovoltage spectroscopy study.

Conflict of Interest: The authors declare no competing financial interest.

Acknowledgment. The work done at KIST was supported by the KIST internal fund, "National Agenda Project" program of Korea Research Council of Fundamental Science & Technology (KRCF), and the Nano·Material Technology Development Program through the National Research Foundation of Korea (NRF) funded by the Ministry of Education, Science and Technology (2012M3A7B4049989). The work done at Green School was supported by the National Research Foundation of Korea Grant funded by the Korean Government (MEST) (2012, University-Institute cooperation program). The work done at SNU was supported by the Global Frontier R&D Program on Center for Multiscale Energy System funded by the National Research Foundation under the Ministry of Education, Science and Technology, Korea (2011-0031574) and by the National Research Foundation of Korea (NRF) grant funded by the Korea government (MEST) (2012-0008669). The authors thank Hye-Eun Nam at Kaywon School of Art & Design for supporting table of contents graphic illustration. The authors also thank Hyeon Ju lee at National Center for Inter-University Research Facilities (NCIRF) for supporting chemical analysis with ESCA spectrometer (SIGMA PROBE).

Supporting Information Available: Additional figures (TEM SAED patterns, pore size distribution, IMPS, and dark-current density). This material is available free of charge *via* the Internet at http://pubs.acs.org.

REFERENCES AND NOTES

1. O'Regan, B.; Gratzel, M. A Low-Cost, High-Efficiency Solar Cell Based on Dye-Sensitized Colloidal TiO_2 Films. *Nature* **1991**, *353*, 737–740.
2. Yella, A.; Lee, H. W.; Tsao, H. N.; Yi, C.; Chandiran, A. K.; Nazeeruddin, M. K.; Diau, E. W. G.; Yeh, C. Y.; Zakeeruddin, S. M.;

Grätzel, M. Porphyrin-Sensitized Solar Cells with Cobalt (II/III)-Based Redox Electrolyte Exceed 12% Efficiency. *Science* **2011**, *334*, 629–634.
3. Sauvage, F.; Decoppet, J. D.; Zhang, M.; Zakeeruddin, S. M.; Comte, P.; Nazeeruddin, M. K.; Wang, P.; Graetzel, M. Effect of Sensitizer Adsorption Temperature on the Performance of Dye-Sensitized Solar Cells. *J. Am. Chem. Soc.* **2011**, *133*, 9304–9310.
4. Tiwana, P.; Docampo, P.; Johnston, M. B.; Snaith, H. J.; Herz, L. M. Electron Mobility and Injection Dynamics in Mesoporous ZnO, SnO_2, and TiO_2 Films Used in Dye-Sensitized Solar Cells. *ACS Nano* **2011**, *5*, 5158–5166.
5. Huang, F.; Chen, D.; Zhang, X. L.; Caruso, R. A.; Cheng, Y. B. Dual-Function Scattering Layer of Submicrometer-Sized Mesoporous TiO_2 Beads for High-Efficiency Dye-Sensitized Solar Cells. *Adv. Funct. Mater.* **2010**, *20*, 1301–1305.
6. Koo, H. J.; Kim, Y. J.; Lee, Y. H.; Lee, W. I.; Kim, K.; Park, N. G. Nano-Embossed Hollow Spherical TiO_2 as Bifunctional Material for High-Efficiency Dye-Sensitized Solar Cells. *Adv. Mater.* **2008**, *20*, 195–199.
7. Liao, J. Y.; Lei, B. X.; Kuang, D. B.; Su, C. Y. Tri-Functional Hierarchical TiO_2 Spheres Consisting of Anatase Nanorods and Nanoparticles for High Efficiency Dye-Sensitized Solar Cells. *Energy Environ. Sci.* **2011**, *4*, 4079–4085.
8. Zhu, K.; Neale, N. R.; Miedaner, A.; Frank, A. J. Enhanced Charge-Collection Efficiencies and Light Scattering in Dye-Sensitized Solar Cells Using Oriented TiO_2 Nanotubes Arrays. *Nano Lett.* **2007**, *7*, 69–74.
9. Robel, I.; Kuno, M.; Kamat, P. V. Size-Dependent Electron Injection from Excited CdSe Quantum Dots into TiO_2 Nanoparticles. *J. Am. Chem. Soc.* **2007**, *129*, 4136–4137.
10. Zhang, Q.; Chou, T. P.; Russo, B.; Jenekhe, S. A.; Cao, G. Aggregation of ZnO Nanocrystallites for High Conversion Efficiency in Dye-Sensitized Solar Cells. *Angew. Chem., Int. Ed.* **2008**, *120*, 2436–2440.
11. Chou, T. P.; Zhang, Q.; Fryxell, G. E.; Cao, G. Hierarchically Structured ZnO Film for Dye-Sensitized Solar Cells with Enhanced Energy Conversion Efficiency. *Adv. Mater.* **2007**, *19*, 2588–2592.
12. Kumar, E. N.; Jose, R.; Archana, P.; Vijila, C.; Yusoff, M.; Ramakrishna, S. High Performance Dye-Sensitized Solar Cells with Record Open Circuit Voltage Using Tin Oxide Nanoflowers Developed by Electrospinning. *Energy Environ. Sci.* **2012**, *5*, 5401–5407.
13. Birkel, A.; Lee, Y. G.; Koll, D.; Van Meerbeek, X.; Frank, S.; Choi, M. J.; Kang, Y. S.; Char, K.; Tremel, W. Highly Efficient and Stable Dye-Sensitized Solar Cells Based on SnO_2 Nanocrystals Prepared by Microwave-Assisted Synthesis. *Energy Environ. Sci.* **2011**, *5*, 5392–5400.
14. Ou, J. Z.; Rani, R. A.; Ham, M. H.; Field, M. R.; Zhang, Y.; Zheng, H.; Reece, P.; Zhuiykov, S.; Sriram, S.; Bhaskaran, M.; *et al*. Elevated Temperature Anodized Nb_2O_5: A Photoanode Material with Exceptionally Large Photoconversion Efficiencies. *ACS Nano* **2012**, *6*, 4045–4053.
15. Tan, B.; Toman, E.; Li, Y.; Wu, Y. Zinc Stannate (Zn_2SnO_4) Dye-Sensitized Solar Cells. *J. Am. Chem. Soc.* **2007**, *129*, 4162–4163.
16. Kim, D. W.; Shin, S. S.; Cho, I. S.; Lee, S.; Kim, D. H.; Lee, C. W.; Jung, H. S.; Hong, K. S. Synthesis and Photovoltaic Property of Fine and Uniform Zn_2SnO_4 Nanoparticles. *Nanoscale* **2012**, *4*, 557–562.
17. Guo, F.; Li, G.; Zhang, W. Barium Staminate as Semiconductor Working Electrodes for Dye-Sensitized Solar Cells. *Int. J. Photoenergy* **2010**, *2010*, 105878.
18. Li, B.; Tang, Y.; Luo, L.; Xiao, T.; Li, D.; Hu, X.; Yuan, M. Fabrication of Porous $BaSnO_3$ Hollow Architectures Using $BaCO_3$@SnO_2 Core−Shell Nanorods As Precursors. *Appl. Surf. Sci.* **2010**, *257*, 197–202.
19. Mizoguchi, H.; Hank, W.; Woodward, P. M. Probing the Electronic Structures of Ternary Perovskite and Pyrochlore Oxides Containing Sn^{4+} or Sb^5. *Inorg. Chem.* **2004**, *43*, 1667–1680.
20. Mizoguchi, H.; Woodward, P. M.; Park, C. H.; Keszler, D. A. Strong Near-Infrared Luminescence in $BaSnO_3$. *J. Am. Chem. Soc.* **2004**, *126*, 9796–9800.
21. Borse, P. H.; Joshi, U. A.; Ji, S. M.; Jang, J. S.; Lee, J. S.; Jeong, E. D.; Kim, H. G. Band Gap Tuning of Lead-Substituted $BaSnO_3$ for Visible Light Photocatalysis. *Appl. Phys. Lett.* **2007**, *90*, 034103.
22. Park, N. G.; Schlichthörl, G.; Van de Lagemaat, J.; Cheong, H.; Mascarenhas, A.; Frank, A. J. Dye-Sensitized TiO_2 Solar Cells: Structural and Photoelectrochemical Characterization of Nanocrystalline Electrodes Formed from the Hydrolysis of $TiCl_4$. *Phys. Chem. B* **1999**, *103*, 3308–3314.
23. Noh, J. H.; Han, H. S.; Lee, S.; Kim, J. Y.; Hong, K. S.; Han, G. S.; Shin, H.; Jung, H. S. Nanowire-Based Three-Dimensional Transparent Conducting Oxide Electrodes for Extremely Fast Charge Collection. *Adv. Energy Mater.* **2011**, *1*, 829–835.
24. Manorama, S.; Reddy, C.; Rao, V. X-Ray Photoelectron Spectroscopic Studies of Noble Metal-Incorporated $BaSnO_3$ Based Gas Sensors. *Appl. Surf. Sci.* **2001**, *174*, 93–105.
25. Sharma, N.; Shaju, K.; Rao, G.; Chowdari, B. Anodic Behaviour and X-Ray Photoelectron Spectroscopy of Ternary Tin Oxides. *J. Power Sources* **2005**, *139*, 250–260.
26. Sargeant, T. D.; Rao, M. S.; Koh, C. Y.; Stupp, S. I. Covalent Functionalization of NiTi Surfaces with Bioactive Peptide Amphiphile Nanofibers. *Biomaterials* **2008**, *29*, 1085–1098.
27. Nazeeruddin, M. K.; Humphry-Baker, R.; Liska, P.; Grätzel, M. Investigation of Sensitizer Adsorption and the Influence of Protons on Current and Voltage of a Dye-Sensitized Nanocrystalline TiO_2 Solar Cell. *J. Phys. Chem. B* **2003**, *107*, 8981–8987.
28. León, C. P.; Kador, L.; Peng, B.; Thelakkat, M. Characterization of the Adsorption of Ru-bpy Dyes on Mesoporous TiO_2 Films with UV-Vis, Raman, and FTIR Spectroscopies. *J. Phys. Chem. B* **2006**, *110*, 8723–8730.
29. Lim, J.; Kwon, Y. S.; Park, S. H.; Song, I. Y.; Choi, J. M.; Park, T. Thermodynamic Control over the Competitive Anchoring of N719 Dye on Nanocrystalline TiO_2 for Improving Photoinduced Electron Generation. *Langmuir* **2011**, *27*, 14647–14653.
30. Kilså, K.; Mayo, E. I.; Brunschwig, B. S.; Gray, H. B.; Lewis, N. S.; Winkler, J. R. Anchoring Group and Auxiliary Ligand Effects on the Binding of Ruthenium Complexes to Nanocrystalline TiO_2 Photoelectrodes. *J. Phys. Chem. B* **2004**, *108*, 15640–15651.
31. Ito, S.; Liska, P.; Comte, P.; Charvet, R.; Péchy, P.; Bach, U.; Schmidt-Mende, L.; Zakeeruddin, S. M.; Kay, A.; Nazeeruddin, M. K. Control of Dark Current in Photoelectrochemical (TiO_2/I^-−I_3^-) and Dye-Sensitized Solar Cells. *Chem. Commun.* **2005**, 4351–4353.
32. Ahmed, S.; Du Pasquier, A.; Asefa, T.; Birnie, D. P., III. Improving Microstructured TiO_2 Photoanodes for Dye-Sensitized Solar Cells by Simple Surface Treatment. *Adv. Energy Mater.* **2011**, *1*, 879–887.
33. Hirose, F.; Kuribayashi, K.; Suzuki, T.; Narita, Y.; Kimura, Y.; Niwano, M. UV Treatment Effect on TiO_2 Electrodes in Dye-Sensitized Solar Cells with N719 Sensitizer Investigated by Infrared Absorption Spectroscopy. *Electrochem. Solid State Lett.* **2008**, *11*, A109.
34. Subramanian, A.; Wang, H. W. Effect of Hydroxyl Group Attachment on TiO_2 Films for Dye-Sensitized Solar Cells. *Appl. Surf. Sci.* **2012**, *258*, 7833–7838.
35. Nelson, J.; Haque, S. A.; Klug, D. R.; Durrant, J. R. Trap-Limited Recombination in Dye-Sensitized Nanocrystalline Metal Oxide Electrodes. *Phys. Rev. B* **2001**, *63*, 205321.
36. Van de Lagemaat, J.; Frank, A. Nonthermalized Electron Transport in Dye-Sensitized Nanocrystalline TiO_2 Films: Transient Photocurrent and Random-Walk Modeling Studies. *J. Phys. Chem. B* **2001**, *105*, 11194–11205.
37. Kim, J. Y.; Noh, J. H.; Zhu, K.; Halverson, A. F.; Neale, N. R.; Park, S.; Hong, K. S.; Frank, A. J. General Strategy for Fabricating Transparent TiO_2 Nanotube Arrays for Dye-Sensitized Photoelectrodes: Illumination Geometry and Transport Properties. *ACS Nano* **2011**, *5*, 2647–2656.
38. Schlichthörl, G.; Huang, S.; Sprague, J.; Frank, A. Band Edge Movement and Recombination Kinetics in Dye-Sensitized Nanocrystalline TiO_2 Solar Cells: A Study by Intensity Modulated Photovoltage Spectroscopy. *J. Phys. Chem. B* **1997**, *101*, 8141–8155.

39. Yum, J. H.; Jang, S.; Humphry−Baker, R.; Grätzel, M.; Cid, J. J.; Torres, T.; Nazeeruddin, M. K. Effect of Coadsorbent on the Photovoltaic Performance of Zinc Pthalocyanine-Sensitized Solar Cells. *Langmuir* **2008**, *24*, 5636–5640.
40. Geiger, T.; Kuster, S.; Yum, J. H.; Moon, S. J.; Nazeeruddin, M. K.; Grätzel, M.; Nüesch, F. Molecular Design of Unsymmetrical Squaraine Dyes for High Efficiency Conversion of Low Energy Photons into Electrons Using TiO_2 Nanocrystalline Films. *Adv. Funct. Mater.* **2009**, *19*, 2720–2727.
41. Zhang, Y.; Zhang, H.; Wang, Y.; Zhang, W. Efficient Visible Spectrum Sensitization of $BaSnO_3$ Nanoparticles with N719. *J. Phys. Chem. C* **2008**, *112*, 8553–8557.
42. Shin, S. S.; Kim, D. W.; Lee, S.; Cho, I. S.; Kim, D. H.; Park, J. H.; Hong, K. S. Surface Modified TiO_2 Nanostructure with 3D Urchin-Like Morphology for Dye-Sensitized Solar Cell Application. *J. Nanosci. Nanotechnol.* **2012**, *12*, 1305–1309.
43. Chandiran, A. K.; Tetreault, N.; Humphry-Baker, R.; Kessler, F.; Baranoff, E.; Yi, C.; Nazeeruddin, M. K.; Grätzel, M. Sub-Nanometer Ga_2O_3 Tunnelling Layer by Atomic Layer Deposition to Achieve 1.1 V Open-Circuit Potential in Dye-Sensitized Solar Cells. *Nano Lett.* **2012**, *12*, 3941–3947.
44. O'Regan, B. C.; Durrant, J. R.; Sommeling, P. M.; Bakker, N. J. Influence of the $TiCl_4$ Treatment on Nanocrystalline TiO_2 Films in Dye-Sensitized Solar Cells. 2. Charge Density, Band Edge Shifts, and Quantification of Recombination Losses at Short Circuit. *J. Phys. Chem. C* **2007**, *111*, 14001–14010.
45. Zhu, K.; Jang, S. R.; Frank, A. J. Impact of High Charge-Collection Efficiencies and Dark Energy-Loss Processes on Transport, Recombination, and Photovoltaic Properties of Dye-Sensitized Solar Cells. *J. Phys. Chem. Lett.* **2011**, *2*, 1070–1076.